Characterization of Standard CMOS Compatible Photodiodes and Pixels for Lab-on-Chip Devices

Gözen Köklü[1,2], Ralph Etienne-Cummings[3], Yusuf Leblebici[2], Giovanni De Micheli[1], and Sandro Carrara[1]

[1]Integrated Systems Laboratory (LSI), Swiss Federal Institute of Technology (EPFL)
[2]Microelectronic Systems Laboratory (LSM), Swiss Federal Institute of Technology (EPFL)
[3]Computational Sensory-Motor Systems Laboratory, Johns Hopkins University (JHU)

***Abstract*—High quality CMOS image sensors are of great importance for LoC - *Lab-on-Chip* devices based on optical measurements. The main target in these devices is to minimize the cost and area while achieving a good resolution. The performance parameters of image sensor pixels and CMOS compatible photodiodes depend on the size, type and the geometry of the photodiode layout and varies for each technology. In this study, we present a comparative analysis of CMOS compatible photodiode types at different areas. The results have shown n-well/p-sub type photodiode with 5×5 μm^2 diffusion area achieves the highest sensitivity (69.81×10^{12} $V.s^{-1}.cm^{-2}/W.cm^{-2}$) and with 40×40 μm^2 diffusion area, highest SNR - *Signal-to-Noise Ratio* ($72.26dB$) at 630 nm, while the p^+/n-well/p-sub type photodiode with 40×40 μm^2 diffusion area results in highest responsivity (0.466 $A.cm^{-2}/W.cm^{-2}$) at the same wavelength.**

I. Introduction

Fluorescence imaging is one of the main analysis methods in today's LoC - *Lab-on-Chip* devices. In the literature, we can find examples of LoC fluorescence devices such as; miniature microscopes for brain imaging of freely moving animals [1], micro-optic/micro-fluidic devices for biochemical analysis [2], and other portable fluorescence detection systems for POC - *Point-of-care* systems for cancer or HIV - *Human Immunodeficiency Virus* diagnostics [3]. LoC devices also find a very wide use in nutrition analysis where the target is mostly to improve health in under-developed or developing countries by offering cheap and effective ways to analyze the food [4].

The main problem in such LoC devices is usually to bring the cost and resolution into a good balance where detailed and robust analysis can be done. For such a system, a very sensitive and high resolution image sensor should be integrated with the LoC device. CMOS technology is a very good candidate for such systems due to its low cost, high integration capabilities and low power. Recently, CMOS image sensors have improved and matured enough to enable a successful integration of the sensor and the LoC devices, while achieving competitive results with the CCDs - *Charge-Coupled Devices* [5]. However, most of the time, these sensors are fabricated by using CIS - *CMOS Image Sensor* dedicated technologies.

The main problems of the dedicated technologies are the availability, cost and the increased complexity which make them disadvantageous especially for research purposes. CIS dedicated/improved technologies are processed by few foundries, where some offer minor improvements by having deeper epitaxial layer, anti-reflective coating and optimization of passivation in order to minimize interference and others provide more dedicated optimizations to improve quantum efficiency and dark current [6]. Moreover, prototyping is only available for large die sizes with a higher cost than standard CMOS processes. Thus, CMOS image sensors fabricated by standard CMOS technologies are better candidates for LoC devices. For a successful integration of a CIS device in a LoC platform, the available photosensors should be well characterized since this data is not given by the foundries. Therefore, the need for characterization of standard CMOS compatible photosensors for each technology always remain and layout optimization and extra layer generation techniques should be further explored in order to improve sensitivity and reach close enough performance results with CIS dedicated technologies.

In this study, we aim to fulfill the need for the characterization data of UMC 0.18μm 6-metal 1-poly standard CMOS process. To the best of our knowledge, this paper presents the first preliminary data in the literature for designers using standard sub-micron CMOS processes for vision chips. Therefore, we provide a quantitative comparison for performance parameters i.e. sensitivity, responsivity and dark noise, of CMOS compatible pixels and photodiode structures with different areas designed in UMC 0.18μm standard CMOS process.

II. CMOS Compatible Pixel Design

Three main photodiode structures i.e. n^+/p-sub, n-well/p-sub, and p^+/n-well/p-sub, are available to be used in standard n-well CMOS processes. *Dark Current*, *Dark Noise*, *Sensitivity* and *Responsivity* are some important parameters that should be characterized when designing a CMOS sensor. These physical parameters depend upon the photodiode structure, geometry, dimensions and the technology.

The literature reports some examples of similar studies that quantitatively compare different photodiode structures where in [7], dimensional effects in different photodiode types are explored for 2μm n-well analog low noise process and in [8], different photodiode structures were compared for a 0.5μm 3-metal, 2-poly, n-well process. However, as mentioned earlier, each of these studies are unique for the process that the sensor is designed with and in both of these processes LOCOS *Local Oxidation* isolation is used where as in sub-micron technologies i.e. *UMC* $0.18\mu m$, STI - *Shallow Trench Isolation* is used which immensely affects photodiode dark noise. Therefore, we provide the characterization data for available photodiodes and

pixels for *UMC* $0.18\mu m$ technology which may be consistent for other sub-micron technologies as well.

A. Performance Parameters of CMOS Photodiodes and Pixels

Sensitivity and *dark current* are the most important parameters in low-light imaging. In the literature, the *sensitivity* parameter of a sensor may be referred in different ways. In this paper, we use *sensitivity* parameter for denoting pixel performance in Volts per unit area and time per incident optical input power per unit area in $V.cm^{-2}.sec^{-1}/W.cm^{-2}$ and *responsivity* parameter for expressing photodiode performance which is defined as the ratio of the photocurrent to the optical input power, in $A.cm^{-2}/W.cm^{-2}$.

Dark current refers to photodiode or pixel leakage current when the sensor is under dark conditions and ideally no photons are entering the device. In this study, we use *dark signal* notation to demonstrate the pixel level leakage signal under dark conditions in mV/sec which is pixel specific but can be used to estimate photodiode *dark current density*.

B. Design of CMOS Photodiodes

The cross section of p^+/n-well/p-sub, n-well/p-sub and n^+/p-sub photodiodes are seen in Fig. 1 and the layouts are drawn by using *Cadence Virtuoso Analog Design Environment*. The metal contacts are placed only on the side of the active areas in order to increase the fill factor and silicide block layer is applied on the diffusion areas with a minimum possible spacing in order to avoid the degradation of the sensitivity due to the opaque silicide layer.

The n^+/p-sub type photodiode is the most straightforward one and achieves the smallest area and second smallest junction capacitance as seen in Table I. It suffers from low collection efficiency due to the highly doped n region and expected to result in low *responsivity* and *sensitivity* compared to the other two structures. The n-well/p-sub type photodiode benefits from the lower doping concentration of n-well, so it achieves higher collection efficiency. However, for the same area of n^+diffusion region, when designed according to the minimum spacing of n-well to n^+, this type photodiode occupies larger area than n^+/p-sub type photodiode. The required spacing of extra well and implant make the area even higher for p^+/n-well/p-sub type photodiode and moreover, the two junction capacitances; p^+ to n-well and n-well to p-sub, are added in parallel and cause the total junction capacitance of this type of photodiode to be much higher than the other types. However, this makes the effective depletion region also much larger and enhances the collection efficiency. Thus, we expect the p^+/n-well/p-sub type photodiode to achieve higher responsivity than the other two, but due to the large junction capacitance, conversion gain will be lower.

C. Pixel Design

The read-out of the corresponding photodiodes mentioned in the previous section are all realized by using traditional three-transistor-type readout circuitry with the same sizing of the transistors. In this architecture, each pixel consists of a reset transistor, source follower and pixel select transistor as seen in Fig. 2a. When the reset signal is active (ϕ_{RS} - High), the photodiode capacitance is pre-charged to some reference level which is depicted as V_{set} and when the ϕ_{RS} signal is low, the

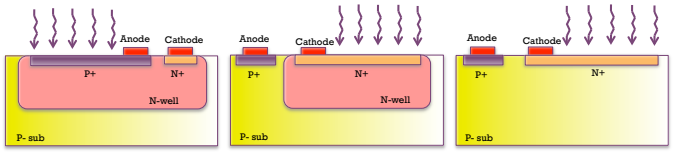

(a) p^+/n-well/p-sub (b) n-well/p-sub (c) n^+/p-sub

Figure 1: Cross Section of Three Different Photodiode Types Compatible with Standard CMOS

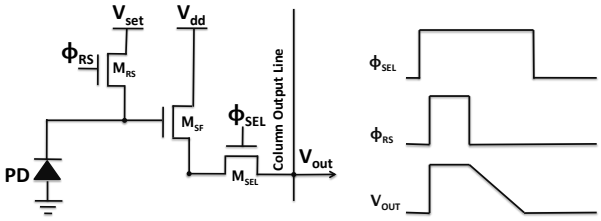

(a) Pixel Schematic (b) Pixel Tran. Behaviour

Figure 2: 3T APS Pixel Schematic and Photodiode Layouts

photocurrent starts to discharge the pre-charged voltage on the photodiode capacitance as seen in Fig. 2b. The output voltage of this circuit can be formalized as below:

$$V_{out} = G_{SF}\frac{1}{C_{PD}}\int I_{PD}\mathrm{dt} \tag{1}$$

where G_{SF} is the source follower gain (common to all pixels), C_{PD} is the photodiode capacitance which is in fact the junction capacitance and I_{PD} is the photodiode current. The junction capacitance can be expressed as below and the required parameters can be found in the model parameters of each design and calculated accordingly:

$$C_{jdep} = \frac{C_{J0}A_D}{(1-(\frac{V_d}{v_j}))^m} + \frac{C_{J0sw}P_D}{(1-(\frac{V_d}{v_{jsw}}))^{m_{jsw}}} \tag{2}$$

where C_{J0} and C_{J0sw} represent zero-bias capacitance at the bottom and sidewall components, V_d is the voltage applied to the photodiode, v_j and v_{jsw} stand for the built-in potential of the bottom and the sidewall respectively, m and m_{jsw} are the grading coefficients of the bottom and the sidewalls, A_D is the photodiode area in m^2 and P_D represents the photodiode perimeter in m. In this equation, we used the same notations for the parameters given in Cadence Spectre Model Parameters and the depletion capacitance can be calculated for each photodiode respectively. Only for the p^+/n-well/p-sub type photodiodes, junction capacitances are calculated by summing the pn junction capacitances; p^+ to n-well and n-well to p-sub. The calculated junction capacitances of the three photodiode structure with different diffusion areas are given on Table I.

III. Experimental Setup

Depending on the required precision of an optical experimental setup, the instruments can become quite costly and bulky. Conversely, we built a very low-cost experimental setup. In this setup, incident light is controlled using an epoxy encased LED - *Light Emitting Diode* together with an ND - *Neutral Density* filter wheel. Light intensity is measured using Thorlabs

Table I: Junction Capacitance (fF) of p^+/n-well/p-sub, n-well/p-sub and n^+/p-sub Type Photodiodes with Different Diffusion Areas

Type	$5x5\mu m^2$	$10x10\mu m^2$	$20x20\mu m^2$	$40x40\mu m^2$
p+/n-well/p-sub	24.37	89.64	367.15	1341.73
n-well/p-sub	2.31	7.84	28.85	110.5
n+/p-sub	19.7	74.6	289.99	1140

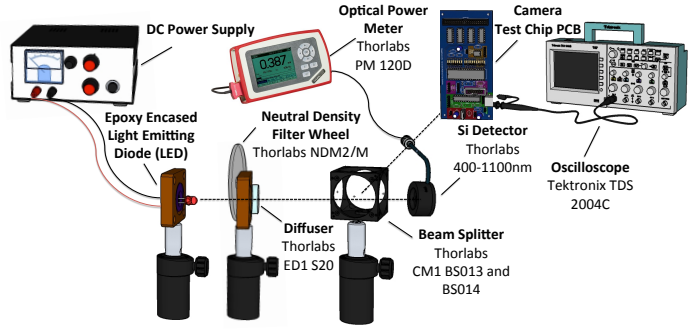

Figure 3: Optical Setup for the Characterization of the CMOS Compatible Photodiodes

optical power meter (PM 120D). Various LEDs at different wavelengths from 465 nm to 940 nm wavelengths are used to cover a wide spectrum which offer a very inexpensive solution compared to spectro-fluorometers and Xenon light sources with controlled spectrums. Moreover, square pattern diffuser is used to increase the uniformity of the generated beam by the LED. Two different cube mounted beam splitters for 400 nm - 700 nm and 700 nm - 1100 nm are used to split the beam equally ("ideally") into two channels where one is connected to the Silicon detector of the optical power meter and the other to the PCB - *Printed Circuit Board* of the test chip. The optical power meter is capable of measuring light sources from 50nW to 50mW at wavelengths between 400 nm to 1100 nm. In this experiment, the voltage output and the corresponding sensitivity, dark signal and SNR with different photodiodes are measured by using 8 bit Tektronix TDS 2004C oscilloscope. The experimental setup is shown in Fig. 3.

IV. Results and Discussion

In this section, we present the measurement results of the test chip in terms of the performance parameters mentioned earlier.

The sensitivity parameter is calculated by normalizing the pixel voltage output discharging slope to the incidence irradiance present on the sensor and the photodiode area. The experiment is repeated for each type of photodiode with different diffusion areas i.e $5\mu m \times 5\mu m$, $10\mu m \times 10\mu m$, $20\mu m \times 20\mu m$ and $40\mu m \times 40\mu m$. Moreover, the data is calculated over a wide spectral range from $465nm$ to $940nm$ by varying the light source among LEDs with different centre wavelengths. The results are shown in separate graphs for each photodiode in Figures 4, 5 and 6.

Responsivity is calculated by multiplying the sensitivity results with the junction capacitance (Eq. 2) of each photodiode as seen in Eq. 1. The results are shown for two different areas of diffusion areas i.e. $5\mu m \times 5\mu m$ and $40\mu m \times 40\mu m$

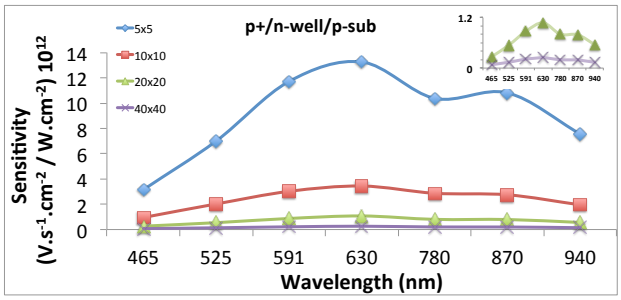

Figure 4: *Spectral Sensitivity* of p^+/n-well/p-sub type photodiodes at different diffusion areas

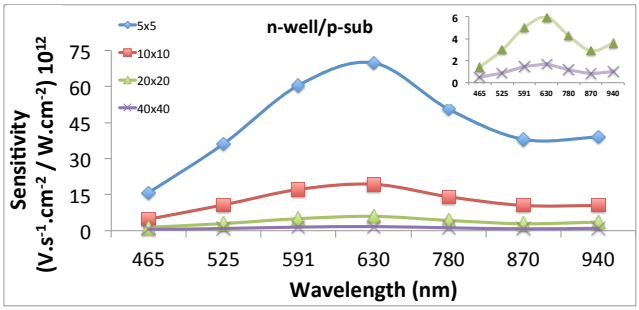

Figure 5: *Spectral Sensitivity* of n-well/p-sub type photodiodes at different diffusion areas

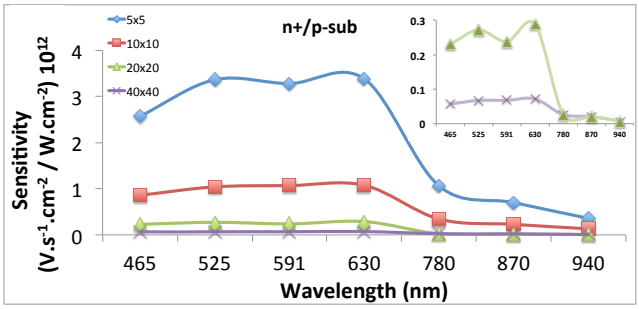

Figure 6: *Spectral Sensitivity* of n^+/p-sub type photodiodes at different diffusion areas

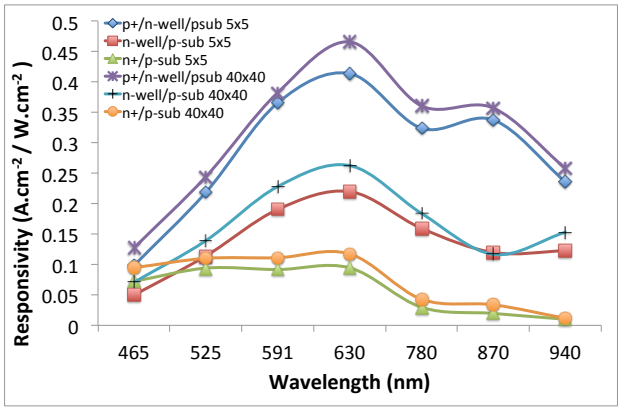

Figure 7: *Responsivity* comparison of different photodiode types at different diffusion areas

and given in Fig. 7. According to these results, p^+/n-well/p-sub type photodiode achieves the highest *responsivity* as expected since the two pn junctions, p^+/n-well and n-well/p-

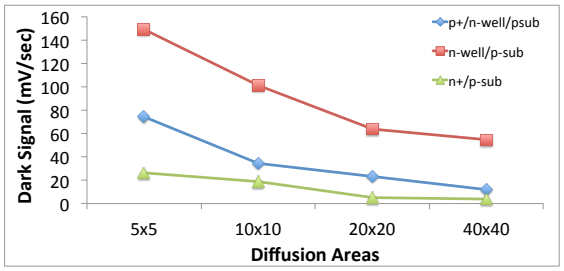

(a) Dark Signal

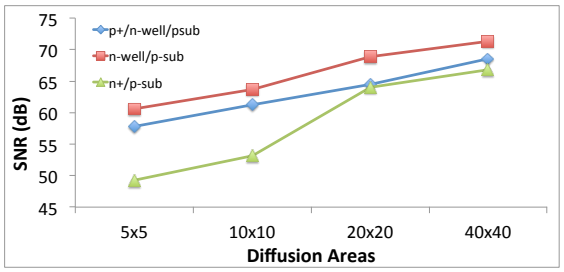

(b) SNR

Figure 8: Comparison of Dark Signal and SNR of Photodiodes with Different Diffusion Areas

sub, increase the collection efficiency. However, as explained earlier, due to the increased junction capacitance of p^+/n-well/p-sub type photodiodes, they result in lower conversion gain and reduced *sensitivity* than pixels with n-well/p-sub type photodiode despite their higher *responsivity*. There results are in accordance with the results shown in paper [1]. Moreover, as expected, as diffusion area is increased, *responsivity* also increases which is due to the fact that the photo carriers generated in the neutral ("dead") regions are also collected by the diffusion [7]. Dark signal is measured by keeping the sensor under dark conditions during a long integration period and the slope of the voltage output under dark conditions is calculated. However, this noise signal is not only due to the photodiode dark current but also partially generated due to the photon shot noise, reset (kT/C) noise and the MOS device noise. In this design, since there are no noise reduction circuits, all the noise sources are present at the output. However, in order to partially remove the shot noise, the collected data is averaged among 128 samples. In Fig. 8a, dark signal dependency over diffusion areas is shown. The decrease of the dark signal by the increase of the photodiode area indicates that the main noise sources contributing to the dark signal is the photodiode dark current and the reset noise since they are both presented at the output with inverse proportionality with the photodiode capacitance. In addition, dark current decreases by the decrease of the reverse bias voltage. However, there is a tradeoff between the dynamic range of the sensor and the reverse bias voltage. In this design, for a good balance between the two, reverse bias voltage, V_{set} in Fig. 2a is set to $1.4V$.

Finally, SNR - *Signal-to-Noise Ratio* parameter provides a relative comparison of the sensitivity and the dark signal. In Fig. 8b, it is shown that SNR increases with the increase of the photodiode area which implies that sensitivity decreases slower than the dark current with respect to photodiode area.

V. CONCLUSION

This comparative study provides preliminary data for CMOS image sensor designers working with UMC $0.18\mu m$ and help them to choose the right diffusion area for the required performance in terms of *responsivity*, *sensitivity* or *SNR* in order to achieve a good balance between resolution, cost and area. The study stresses the dimensional effects on CMOS compatible photodiode structures and recommends the use of n-well/p-sub type photodiodes for higher sensitivity and SNR results while achieving lower area than p^+/n-well/p-sub type photodiodes. n^+/p-sub type photodiodes have the smallest area but due to 20 times less sensitivity and 2 times less responsivity than n-well/p-sub type photodiodes and 4 times less sensitivity and responsivity than p^+/n-well/p-sub type photodiodes, n^+/p-sub type photodiode is out of discussion for low light imaging applications. Finally, for LoC devices targeting fluorescence imaging, we recommend a careful selection of fluorophores since the fluorophores emitting light at wavelengths from 630 nm to 780 nm reach highest *responsivity* and *sensitivity*.

ACKNOWLEDGMENT

The research work presented in this paper was funded by the NutriCHIP project with a grant from the Swiss Nano-Tera.ch initiative, evaluated by the Swiss National Science Foundation. It was also partially supported by the NanoSys project (program ERC-2009-AdG-246810). Finally, the authors would like to thank to Garrick Orchard from Computational Sensory-Motor Systems Laboratory at Johns Hopkins University for the valuable help during PCB preparation and configuration.

REFERENCES

[1] K. Murari, R. Etienne-Cummings, G. Cauwenberghs and N. Thakor, *An integrated imaging microscope for untethered cortical imaging in freely-moving animals* Conf. Proc. IEEE Eng. Med. Biol. Soc., pp.5795-5798, 2010.

[2] J.C. Roulet, R. Völikel, H.P. Herzig, E. Verpoorte, N.F de Rooij, and R. Dandliker *Performance of an Integrated Microoptical System for Fluorescence Detection in Microfluidic Systems*, Anal. Chem. 2002 74 (14), 3400-3407.

[3] B. Zhang, Z. Li, Q. Yuan, C. Chang, M.E. Zaghloul, *Point-of-care early HIV diagnosis system on the CMOS & microfluidic hybrid platform,* Biomedical and Health Informatics (BHI), 2012 IEEE-EMBS Int. Conf. on, vol., no., pp.624-627, 5-7 Jan. 2012.

[4] G. Vergeres, B. Bogicevic, C. Buri, S. Carrara, M. Chollet, L. Corbino-Giunta, L. Egger, D. Gille, K. Kopf-Bolanz, K. Laederach, R. Portmann, Q. amadan, J. Ramsden, F. Schwander, P. Silacci, B. Walther and M. Gijs. *The NutriChip project - translating technology into nutritional knowledge*. British J. of Nutrition, 108 , pp 762-768.

[5] G. Koklu, J. Ghaye, R. Beuchat, G. De Micheli, Y. Leblebici, S. Carrara, *Quantitative comparison of commercial CCD and custom-designed CMOS camera for biological applications*, Circuits and Systems (ISCAS), 2012 IEEE Int. Sym. on, vol., no., pp.2063-2066, 20-23 May 2012.

[6] P. Martin-Gonthier, P. Magnan and F. Corbiere, *Overview of CMOS process and design options for image sensor dedicated to space applications*, Proc SPIE, vol. 5978, pp. 597812, 2005

[7] I. Brouk and Y. Nemirovsky, *Dimensional effects in CMOS photodiodes*, Solid-State Electronics 46- 2002) 19-28.

[8] K. Murari, R. Etienne-Cummings, N. Thakor and G. Cauwenberghs *Which Photodiode to Use: A Comparison of CMOS-Compatible Structures*, IEEE Sensors J., Vol. 9, No. 7, July 2009.

[9] A. Pauchard, P.-A. Besse, and R. S. Popovic, *A silicon blue/UV selec- tive stripe-shaped photodiode* Sens. Actuators, vol. 76, pp. 172-177, 1999.

[10] A. Pauchard, *Silicon Sensor Microsystem for Ultraviolet Detection*, ser. Microsystems. Konstanz, Germany: Hartung Gorre Verlag, 2000, vol. 7.

[11] A. Ghazi, H. Zimmermann and P. Seegebrecht, *CMOS Photodiode With Enhanced Responsivity for the UV/Blue Spectral Range*, IEEE Tran. on Elect. Dev., Vol. 49, No. 7, July 2002.